Asian Journal of Chemistry; Vol. 34, No. 6 (2022), 1383-1390

ASIAN JOURNAL OF CHEMISTRY

https://doi.org/10.14233/ajchem.2022.23626

Synthesis, Characterization, Electrochemical and Anitmicrobial Studies of Manganese(IV) Complexes Derived from Polyfunctional Glutaryldihydrazone

P. SARMA[1], P. MAHANTA[1], D. BASUMATARY[1,*] and C. MEDHI[2]

[1]Department of Applied Sciences, Gauhati University, Guwahati-781014, India
[2]Department of Chemistry, Gauhati University, Guwahati-781014, India

*Corresponding author: Tel: +91 361 2570412; E-mail: debbasumatary@gmail.com; debbasumatary@gauhati.ac.in

Received: 22 November 2021; *Accepted*: 15 January 2022; *Published online*: 18 May 2022; AJC-20796

The synthesis and structure elucidation of a new series of manganese(IV) complexes from disalicylaldehyde glutaryldihydrazone ($slghH_4$) of the composition $[Mn^{IV}(slgh)](A)_2]\cdot H_2O$ and $[Mn^{IV}(slgh)(NN)]$ (where A= H_2O, (**1**); pyridine, (**2**); 2-picoline, (**3**); 3-picoline, (**4**); 4-picoline, (**5**) and NN = 2,2′-bipyridine, (**6**); 1,10-phenanthroline, (**7**)) were carried out. The composition and structures of all the complexes of Mn(IV) have been evaluated by elemental analysis, thermal studies, molar conductance, mass spectral data, magnetic moment, electronic, electron paramagnetic resonance and infrared spectral studies. Molar conductances of these Mn(IV) complexes suggest their non-electrolytic nature. Magnetic moment and EPR studies suggested that the Mn(IV) ions are six-coordinated octahedral geometry around the metal ions. The IR spectral studies confirmed that the ligand coordinates to the Mn(IV) ion in enolic form and behave as a tetradentate ligand in *anti-cis* configuration chelating Mn(IV) ion with NNOO coordination sites. The electrochemical and antimicrobial studies of the Mn(IV) complexes have also been carried out.

Keywords: Disalicylaldehyde glutaryldihydrazone, Manganese(IV), Stereochemistry, Redox activity, Antimicrobial activity.

INTRODUCTION

Hydrazone Schiff bases are a class of compounds that constitute azomethine linkage (C=N) and are widely used in the field of coordination chemistry. In coordination chemistry, metal complexes of aroylhydrazone ligands have gained significant interest due to their versatility and ability to generate different molecular geometries since many of these complexes serve as a model for biological systems [1,2]. Hydrazones have shown the keto-enol (amido-iminol) tautomerism and can coordinate in neutral, monoanionic or dianionic forms to metal ions with a broad diversity of coordination numbers [3].

Hydrazones are also called versatile ligands as they can coordinate with various metal ions in several oxidation states and geometries and turn as remarkable chelating agents due to the presence of nitrogen, oxygen or sulphur [4]. Over the past few years, hydrazone ligands have attracted much attention from researchers because of their well-known chelating capability and structural flexibility and they constitute ONO and NNO donor atoms that have been introduced to coordination chemistry [5-7]. Hydrazones have a broad range of physiological and biological activities such as anticancer, antibacterial, antioxidant, antifungal, antitubercular, anti-inflammatory, antiviral and antipyretic properties [8-10]. Hydrazones also play an important role in improving the antitumor selectivity and toxicity profile of antitumor agents by forming drug carrier systems employing suitable carrier proteins and have also been used as analytical reagent, polymer-coating, ink, pigment and fluorescent materials [11,12].

The chemistry of manganese in a high oxidation state is a subject of particular interest due to its occurrence in many biological systems *e.g.* in superoxide dismutase, an azide insensitive catalase and photosystem-II (PS-II) [13,14]. Manganese complexes in a high-oxidation state are potentially used as oxidizing agents, catalysts and electrocatalysts for oxidation of alcohols, ethers and water [15,16]. Moreover, it occurs in enzymes, some multinuclear enzymes like arginase that requires manganese to perform their biological activity. The manganese has to play a crucial role in the natural ecosystem and is known to be a key player in the water oxidation process, which occurs

during the natural photosynthesis [17-20]. Thus, the importance of manganese in many biological systems has stimulated the study of chemistry of manganese(II), manganese(III), manganese(IV) and manganese(V) with variable nuclearity [19]. In present study, we have designed hydrazone Schiff bases that constitute NNOO architecture to bind the metal ions. Because of the significant role played by manganese and a less work with a high oxidation state of manganese, we have carried out the work. Moreover, the absence of work on metal complexes of the title dihydrazone has intrigued us to pursue the work further. Herein, we have reported the synthesis, spectroscopic characterization, electrochemical behaviour and antimicrobial activity of disalicylaldehyde glutaryldihydrazone and its manganese(IV) complexes.

EXPERIMENTAL

Manganese acetate ($Mn(OAc)_2{\cdot}4H_2O$), diethyl glutarate, hydrazine hydrate ($N_2H_4{\cdot}H_2O$) and salicylaldehyde were E-Merck or equivalent grade reagents.

Determination of manganese has been done by following the standard procedure [21]. Carbon, hydrogen and nitrogen contents were microanalytically estimated using Euro EA elemental analyzer. Room temperature magnetic susceptibility measurements have been performed on a Sherwood scientific magnetic susceptibility balance using $Hg[Co(SCN)_4]$ as calibrant. Molar conductances of the ligand and its metal complexes were carried out in DMSO (~ 10^{-3} M) on a Systronics Direct Reading Conductivitymeter-303 with dip-type conductivity cell at room temperature. Infrared spectra were recorded on a Spectrum2 Perkin-Elmer FTIR spectrometer in KBr disks. Electronic spectra of the ligand and its complexes have been studied from 250 to 800 nm in DMSO on a Perkin-Elmer Lambda 35 UV-vis spectrophotometer. EPR spectra of the complexes as powders as well as in DMSO were recorded at X-band frequency on JES-FA200 ESR spectrometer at liquid nitrogen temperature (LNT) and room temperature (RT). LC-MS spectra of the complexes were recorded on UHPLC-Ultimate 3000, Thermo scientific, MS-Exactive Plus spectrometer. Melting point and decomposition temperatures were obtained using Analab Scientific instruments. Thermal stability and decomposition of the analytical complexes were performed by means of Mettler-Toledo thermal analyzer system recording TGA and DTG curves in the temperature range 25-700 ºC under N_2 atmosphere with a heating rate of 20 ºC min^{-1}. Studies with cyclic voltammetry were performed using CHI660D CH instrument electrochemical workstation using TBAP as supporting electrolyte under nitrogen atmosphere. The electrolytic cell comprised of three electrodes, the working electrode was a Pt disk, while the reference electrode was Ag/AgCl and an auxiliary electrode was Pt wire.

Synthesis of ligand: Glutarohydrazide is prepared by the condensation of diethyl glutarate (5.11 g, 27 mmol) with hydrazine hydrate (3.087 g, 61 mmol) in a 1:2 molar ratio. Disalicylaldehyde glutaryldihydrazone was then prepared by reacting glutarohydrazide (1.6 g, 10 mmol) with salicylaldehyde (2.13 mL, 20 mmol) in ethanol at room temperature under reflux for 0.5 h. The white precipitate was thoroughly washed with hot methanol, filtered and air-dried (decomposition point > 250 ºC).

Synthesis of complex $[Mn^{IV}(slgh)(H_2O)_2]{\cdot}H_2O$ (1): Manganese acetate ($Mn(OAc)_2{\cdot}4H_2O$) (0.245 g, 1 mmol) in methanol (15 mL) was allowed to react with ligand ($slghH_4$) (0.368 g, 1 mmol) in 25 mL methanol in 1:1 molar ratio stirred for 30 min at room temperature. The resulting solution was then refluxed for 2 h. The precipitated pale yellow coloured complexes were filtered, washed several times with hot methanol and dried over anhydrous $CaCl_2$ (Yield = 78 %).

Synthesis of complexes $[Mn^{IV}(slgh(A)_2)].nH_2O$ and $[Mn^{IV}(slgh)(NN)]$ (where A= pyridine (py, 2); 2-picoline (2-pic, 3); 3-picoline (3-pic, 4) and 4-picoline (4-pic, 5) and NN = 2,2′ bipyridine (bpy, 6) and 1,10-phenanthroline (phen, 7)): These complexes were also synthesized by following the above mentioned procedure and adding pyridine bases to the reaction mixture obtained by mixing $Mn(OAc)_2{\cdot}4H_2O$ and $slghH_4$ maintaining $Mn(OAc)_2{\cdot}4H_2O$: $slghH_4$:pyridine molar ratio at 1:1:10 in case of pyridine bases and 1:1:2 in case of 2,2′-bipyridine and 1,10-phenanthroline. Yield: 64% (**2**); 69% (**3**); 57% (**4**), (**5**); 68% (**6**) and 72 % (**7**).

Antimicrobial studies: The efficiencies of the ligand and its four manganese complexes (**2**, **3**, **6** and **7**) were tested for antimicrobial activity against bacteria *viz*. *Staphylococcus epidermis*, *Bacillus cereus*, *Escherichia coli* and *Proteus vulgaris* by standard Agar well diffusion method [22]. An overnight culture of indicator strain *Staphylococcus epidermis*, *Bacillus cerus*, *Escherichia coli* and *Proteus vulgaris* were used to inoculate in Muller Hinton Agar as 0.5 McFarland standard. Wells of 8 mm diameter were cut into agar plates and 50 µL of the sample was added to each well. Inhibitory zone was checked after 24 h incubation at 37 ºC.

RESULTS AND DISCUSSION

The synthesized manganese(IV) complexes with their composition, colour, decomposition point, analytical, magnetic moment and molar conductance data are given in Table-1. The complexes are air-stable and insoluble in water and most common organic solvents such as ethanol, acetone, *etc*. but dissolved freely in coordinating solvents like DMSO and DMF. The complexes decomposed above 250 ºC indicating strong bonding. The synthesized manganese(IV) complexes (**1-5**) show weight loss at 110 ºC that indicates that there is water in the lattice structure [23], while complex **1** also shows loss corresponding to two water molecules at 180 ºC, indicating they are coordinated to the metal [24]. Complexes (**2-7**) also showed a weight loss at 220 ºC associated with two pyridine or substituted pyridine molecules while the complexes **6** and **7** show the weight loss corresponding to one bipyridine and one 1,10-phenanthroline, respectively. We were unable to crystallize these complexes which prevented us from the analysis of the complexes by X-ray crystallography to establish their molecularity and structure.

Thermal studies: The complexes do not decompose up to the observed temperature range of 250 ºC that indicates the strong metal-ligand bonds with higher ionic character. The complexes **1** and **3** were studied as representative samples by

TABLE-1
COLOUR, DECOMPOSITION POINT, ANALYTICAL, MAGNETIC MOMENT AND MOLAR CONDUCTANCE DATA FOR Mn(IV) COMPLEXES OF DISALICYLALDEHYDE GLUTARYLDIHYDRAZONE ($slghH_4$)

Complex	Colour	Decomp. temp. (°C)	Elemental analysis (%): Found (calcd.)				μ_{eff} (B.M)	Molar conductance (Λ_m) (ohm^{-1} cm^2 mol^{-1})
			Mn	C	H	N		
$[Mn^{IV}(slgh)(H_2O)_2]\cdot H_2O$	Pale yellow	> 250	11.95 (12.08)	50.36 (50.10)	4.48 (4.39)	11.56 (12.30)	4.22	1.9
$[Mn^{IV}(slgh)(py)_2]\cdot H_2O$	Pale yellow	> 250	9.27 (9.53)	60.19 (60.31)	4.59 (4.50)	14.17 (14.55)	4.30	2.5
$[Mn^{IV}(slgh)(2\text{-}pic)_2]\cdot H_2O$	Pale yellow	> 250	9.01 (9.09)	57.68 (61.48)	4.54 (4.95)	12.28 (13.88)	4.20	2.3
$[Mn^{IV}(slgh)(3\text{-}pic)_2]\cdot H_2O$	Yellow	> 250	9.20 (9.09)	58.09 (61.48)	4.63 (4.95)	13.17 (13.88)	4.30	2.2
$[Mn^{IV}(slgh)(4\text{-}pic)_2]\cdot H_2O$	Pale yellow	> 250	9.11 (9.09)	56.87 (61.48)	4.73 (4.95)	13.09 (13.88)	4.13	2.8
$[Mn^{IV}(slgh)(bpy)]$	Pale yellow	> 250	9.31 (9.56)	58.79 (60.52)	4.44 (4.17)	13.49 (14.60)	4.27	1.5
$[Mn^{IV}(slgh)(phen)]$	Pale yellow	> 250	8.87 (9.18)	57.93 (62.10)	4.61 (4.01)	13.61 (14.02)	4.19	2.1

thermogravimetric analysis. Thermogravimetric studies of complexes **1** and **3** showed that both complexes decomposed in six stages. In first stage, the TGA/DTG curve of complex **1** exhibited degradation within the temperature range of 30-132 ºC with a DTG peak at 42 °C (Fig. 1). The corresponding weight loss of 3.49% (calcd. 3.81%) was suggested to be due to the weight loss of one lattice water molecule. The second stage degradation within the temperature range of 132-298 ºC with DTG peak at 222 ºC and weight loss of 4.04% (calcd. 3.96%) attributed to the release of one coordinated water molecule. In the third stage, corresponding weight loss of 35.46% (calcd. 36.17%) decomposition occurred between 298-414 ºC with associated DTG peak that was observed at 379 ºC due to the loss of another coordinated water molecule and an organic ($C_4H_4O_2N_4$) moiety. With a weight loss of 9.58% (calcd. 9.68%) in the fourth degradation stage within the temperature range, 414-468 ºC that corresponds to the discharge of ($-C_2H_3$) molecule with associated DTG peak that was observed at 431 ºC. The release of ($-C_2H_4$) fragments with DTG peak at 510 ºC in the fifth stage exhibited one degradation observed between 468-580 ºC with a weight loss of 10.88% (calcd. 11.12%). The sixth degradation stage showed weight loss of 5.33% (calcd. 5.81%) that occurred between 580-686 ºC associated with the DTG curve that was observed at 653 ºC attributed to the loss of (-CH) moiety. The overall weight loss is 68.78% against the calculated value of 70.55%.

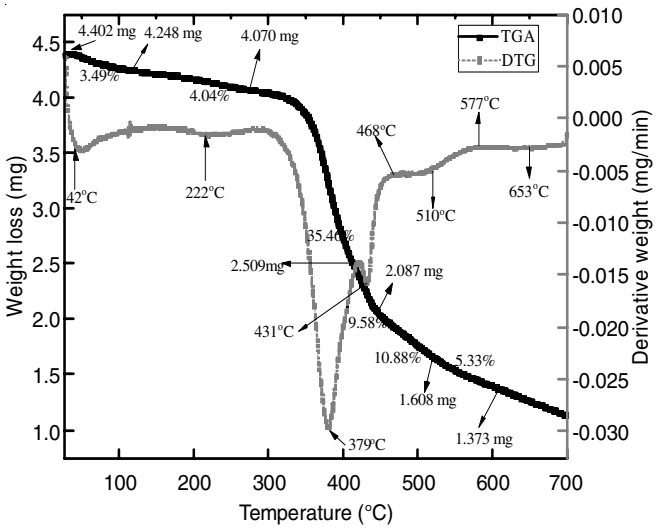

Fig. 1. TGA and DTG curves of $[Mn^{IV}(slgh)(H_2O)_2]\cdot H_2O$ (**1**)

The thermogram of complex **3** exhibited the first decomposition stage within the temperature range between 29-96 ºC associated with a DTG peak centered at 58 ºC and weight loss of 2.66% (calcd. 2.89%), which correspond to the discharge of one lattice H_2O molecule. The second degradation stage shows a weight loss of 2.37% (calcd. 2.48%) that occurred at 151-225 ºC and corresponds to the liberation of ($-CH_3$) moieties with the DTG peak that is observed at 192 ºC. The third stage proceeded with a weight loss of 2.46% (calcd. 2.55%) in the temperature range 228-288 ºC with a DTG peak at 245 °C that corresponds to the removal of another ($-CH_3$) moieties. The combined weight losses of 41.46% (calcd. 42.12%) in the fourth degradation stage occurred within the temperature ranges of 299-442 ºC attributable to the simultaneous losses of two pyridine moieties and another ($-C_4H_5O_2$) moiety with DTG peak centered at 428 ºC. The fifth and sixth decomposition stages observed between the temperature ranges of 442-482 ºC and 501-616 ºC and the corresponding weight losses of 9.11% (calcd. 8.99%) and 9.41% (calcd. 9.55%) followed by the DTG peak observed at 447 ºC and 565 ºC are due to the losses of ($-C_2H_6$) and ($-C_2H_5$) moieties, respectively.

The overall weight loss of 67.47% (calcd. 68.58%) was estimated between the temperature range of 29-616 ºC. The stages of thermal decomposition and the percentage loss of masses along with their assigned molecules/fragments are shown in Table-2. These thermal investigations indicated the presence of one water molecule in the lattice of complexes (**1** and **3**) and also two coordinated water molecules in the structure of complex **1**, which are in good agreement with their IR spectral studies [5,25].

Molar conductance: The molar conductance values for complexes are shown in Table-1. The values lie in the range 1.9-2.8 ohm^{-1} cm^2 mol^{-1} in DMSO that indicate their non-electrolytic nature in this solvent [26].

Mass spectra: The mass spectrum of ligand $slghH_4$ exhibits a signal at $m/z = 369$, which corresponds to the formula weight of the ligand. A signal observed at $m/z = 367$ in complex **1** corresponds to the formation of the species $[slghH_2]^+$ formed after the loss of the manganese atom. Another signal in this complex at $m/z = 407$ may be due to the loss of CH_2 molecule and two water molecules with the formation of $[C_{18}H_{14}N_4O_4Mn]^+$ species.

Magnetic moment: The μ_B values for the synthesized manganese(IV) complexes are shown in Table-1. These values

TABLE-2
THERMOANALYTICAL RESULTS (TG AND DTG) OF MANGANESE(IV) COMPLEXES OF $slghH_4$

Complexes	TG range (°C)	DTG (°C)	Found (calcd.)%		Assignment
			Mass loss	Total mass loss	
$[Mn^{IV}(slgh)(H_2O)_2]\cdot H_2O$ (**1**)	30-132	42	3.49 (3.81)	68.78 (70.55)	Loss of one lattice H_2O molecule
	132-298	222	4.04 (3.96)		Loss of one coordinated H_2O molecule
	298-414	379	35.46 (36.17)		Loss of one coordinated water molecule & ($-C_4H_4O_2N_4$)
	414-468	431	9.58 (9.68)		Loss of organic moiety ($-C_2H_3$)
	468-580	510	10.88 (11.12)		Loss of organic moiety ($-C_2H_4$)
	580-686	653	5.33 (5.81)		Loss of organic moiety (-CH)
$[Mn^{IV}(slgh)(2\text{-}pic)_2]\cdot H_2O$ (**3**)	29-96	58	2.66 (2.89)	67.47 (68.58)	Loss of one lattice H_2O molecule
	151-225	192	2.37 (2.48)		Loss of organic moiety ($-CH_3$)
	228-288	245	2.46 (2.55)		Loss of organic moiety ($-CH_3$)
	299-442	428	41.46 (42.12)		Loss of two pyridine base molecules & ($-C_4H_5O_2$)
	442-482	447	9.11 (8.99)		Loss of organic moiety ($-C_2H_6$)
	501-616	565	9.41 (9.55)		Loss of organic moiety ($-C_2H_5$)

lie in the range 4.1-4.3 B.M., which fall within the range reported for Mn(IV) in a d^3 high spin electronic configuration ruling out the possibility of any spin-spin coupling in the solid-state between unpaired electrons belonging to different Mn(IV) centers in structural unit of the complexes [27-29].

Electronic spectra: The electronic spectral bands for dihydrazone and metal complexes are listed in Table-3 along with their molar extinction coefficients. The electronic absorption spectra of the ligand and complexes are shown in Fig. 2. The absorption spectrum of free dihydrazone is characterized by two bands at 292 (7741) and 322 (6365) nm, which arise from π-π* and n-π* transitions. In metal complexes, these bands are observed as one to two bands with both red and blue shifts. In complexes **1-7**, the ligand band observed at 292 nm undergoes almost no shift or a slight red shift by 1-6 cm^{-1}. Another ligand band at 322 nm in the complexes **2-5** undergo blue shift by 10-19 cm^{-1} with decrease in intensity while this ligand band in complexes **6** and **7** undergoes slight red by 1-2 cm^{-1}. In addition to ligand bands, the complexes possess an additional band in the region 387-402 nm. This provides good evidence for chelation by dihydrazone to the metal center. The magnitude of shift of ligand bands on complexation indicates

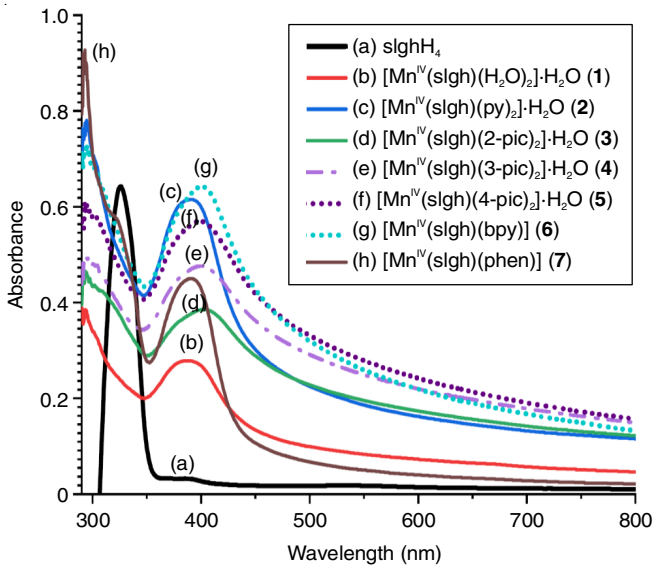

Fig. 2. Electronic spectra of ligand (a) $slghH_4$ and complexes (b) $[Mn^{IV}(slgh)(H_2O)_2]\cdot H_2O$ (**1**), (c) $[Mn^{IV}(slgh)(py)_2]\cdot H_2O$ (**2**), (d) $[Mn^{IV}(slgh)(2\text{-}pic)_2]H_2O$ (**3**), (e) $[Mn^{IV}(slgh)(3\text{-}pic)_2]\ H_2O$ (**4**), (f) $[Mn^{IV}(slgh)(4\text{-}pic)_2]H_2O$ (**5**), (g) $[Mn^{IV}(slgh)(bpy)]$ (**6**), (h) $[Mn^{IV}(slgh)(phen)]$ (**7**)

TABLE-3
ELECTRONIC SPECTRAL BANDS AND EPR DATA FOR MANGANESE(IV) COMPLEXES OF $slghH_4$

Ligand/Complex	λ_{max}, nm (ε_{max}, $dm^3\ mol^{-1}\ cm^{-1}$)	Temp.	Solid/solution	g-Value	A_{Mn} value
$slghH_4$	292 (7741), 322 (6365)				
$[Mn^{IV}(slgh)(H_2O)_2]\cdot H_2O$	290 (3884), 387 (2789)	LNT	DMSO	2.014	98
		RT	DMSO	2.1	99
		RT	SOLID	2.045	
$[Mn^{IV}(slgh)(py)_2]\cdot H_2O$	294 (7816), 303 (6898), 390 (6202)	LNT	DMSO	2.01	96
		RT	DMSO	2.1	96
		RT	SOLID	2.045	
$[Mn^{IV}(slgh)(2\text{-}pic)_2]\cdot H_2O$	293 (4590), 312 (4205), 402 (3865)	LNT	DMSO		
		RT	DMSO		
		RT	SOLID	2.045	
$[Mn^{IV}(slgh)(3\text{-}pic)_2]\cdot H_2O$	298 (4926), 310 (4541), 400 (4782)				
$[Mn^{IV}(slgh)(4\text{-}pic)_2]\cdot H_2O$	293 (5984), 304 (5744), 402 (5974)				
$[Mn^{IV}(slgh)(bpy)]$	296 (7190), 324 (5670), 401 (6420)	LNT	DMSO		
		RT	DMSO		
		RT	SOLID	2.045	
$[Mn^{IV}(slgh)(phen)]$	293 (9270), 323 (5769), 391 (4520)	LNT	DMSO		
		RT	DMSO		
		RT	SOLID	2.045	

strong bonding between the ligand and the metal center. The high molar extinction coefficient values in these Mn(IV) complexes may be assigned to charge-transfer with large contribution from ligand-to-metal charge transfer [28-32].

EPR spectra: The EPR magnetic parameters for the synthesized Mn(IV) complexes are given in Table-3. EPR spectra of the complexes in solid state at RT are essentially similar to one another and show an isotropic signal with g = 2.045. On the other hand, in DMSO at RT and LNT, six-line spectra are obtained with ^{55}Mn hyperfine splitting constant falling in the range 96-99 G for complexes **1** and **2** taken as representative samples. This ^{55}Mn hyperfine splitting constant is characteristic of Mn(IV) complexes rather than for Mn(II) complexes. The overall intensity of split components of the signal due to ^{55}Mn hyperfine splitting at LNT and RT in DMSO is weak for complex **2** as compared to that of complex **1**. The well-resolved superhyperfine lines due to hidden transitions are observed for complex **1** at LNT in DMSO, which are weak in the ESR spectrum of complex **2** at RT in DMSO. An effective environment of Mn(IV) is suggested to lie close to ideally pseudo-octahedral environment [24,32,33].

IR spectra: Some structurally significant IR bands for free dihydrazone and their metal complexes are given in Table-4. The IR spectra for dihydrazone and complexes **1** and **2** are shown in Fig. 3. IR spectral bands for the dihydrazone show medium to strong intensity bands in the region centered at 3440, 3193 and 3056 cm^{-1} that are assigned to the stretching vibrations of phenolic –OH and secondary –NH group [34]. In the complexes, the above bands are replaced by broad bands in the region 3600-3000 cm^{-1}. Such a feature of IR spectra is associated with the destruction of -NH group on complexation [35]. A strong band at 1668 cm^{-1} in the free dihydrazone is assignable to stretching frequency νC=O band [24,26]. The carbonyl bands disappear in complexes indicating the collapse of amide structure and coordination of ligand to the metal in

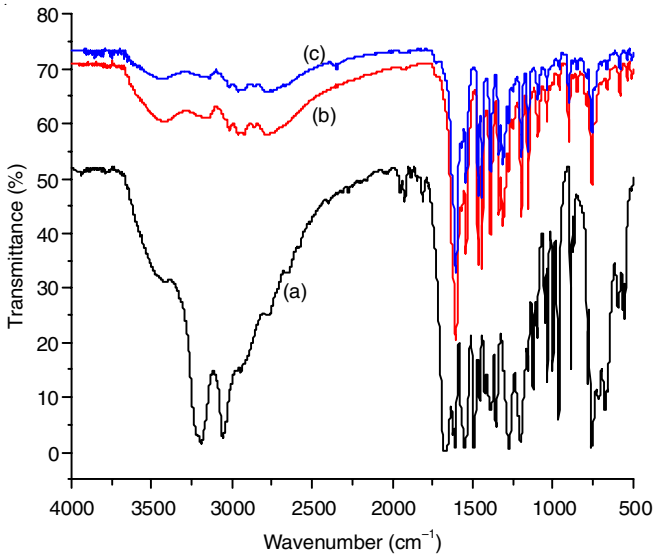

Fig. 3. Infrared spectra of ligand (a) slghH$_4$ and complexes (b) [Mn^{IV}(slgh)(H$_2$O)$_2$]·H$_2$O (**1**), (c) [Mn^{IV}(slgh)(py)$_2$]·H$_2$O (**2**)

enolic form. This also dismisses the possibility of coordination of >NH and >C=O groups to the metal center. The two strong intensity bands observed at 1623 and 1611 cm^{-1} in the free dihydrazone are assignable to ν(C=N) bands [36]. These bands appear as single bands in the complexes and on an average shift to a lower frequency by 9-16 cm^{-1} indicating coordination of >C=N group to the metal centre [28,37]. The appearance of merged ν(C=N) bands is still related to arise due to the coordination of both the azomethine nitrogen atoms and phenolate oxygen atoms of the same dihydrazone molecule to the same metal center. A medium to weak intensity band appearing at 585-580 cm^{-1} is assigned to ν(M-O) (phenolic) that indicates the π-electron density flow of aromatic ring to the metal center through phenolic oxygen atoms [38]. Pyridine bases absorb at around ~604 cm^{-1} due to in-plane ring deformation mode [24].

TABLE-4
STRUCTURALLY SIGNIFICANT INFRARED SPECTRAL BANDS OF slghH$_4$ AND ITS MONOMETALLIC Mn(IV) COMPLEXES

Ligand/Complex	ν(OH) + ν(NH)	ν(C=O)	ν(C=N)	Amide(II) + ν(CO) phenolic	ν(C-O) (phenolic)	ν(N-N)	ν(Mn-O) phenolic	ν(Mn-N) py/bpy/phen vibration in plane
slghH$_4$	3000-3600(sbr) 3440(m) 3193(s) 3056(s)	1668(s)	1623(s) 1611(s)	1554(s)	1275(s)	1040(s) 1036(s)		
[Mn^{IV}(slgh)(H$_2$O)$_2$]·H$_2$O	3000-3600(mbr) 3440(m)	–	1601(s)	1543(s)	1274(w)	1042(m)	585(m)	–
[Mn^{IV}(slgh)(py)$_2$]·H$_2$O	3000-3600(mbr) 3440(m)	–	1608(s)	1543(s)	1273(w)	1042(m)	585(w)	665(m)
[Mn^{IV}(slgh)(2-pic)$_2$]·H$_2$O	3000-3600(mbr) 3429(m)	–	1601(s)	1543(s)	1274(w)	1042(m)	585(w)	665(w)
[Mn^{IV}(slgh)(3-pic)$_2$]·H$_2$O	3000-3600(mbr) 3420(m)	–	1601(s)	1543(s)	1277(w)	1042(m)	585(w)	664(w)
[Mn^{IV}(slgh)(4-pic)$_2$]·H$_2$O	3000-3600(mbr) 3422(m)	–	1602(s)	1543(s)	1273(w)	1042(m)	585(m)	665(w)
[Mn^{IV}(slgh)(bpy)]	3000-3600(mbr) 3426(m)	–	1601(s)	1543(s)	1276(w)	1042(w)	585(m)	665(w)
[Mn^{IV}(slgh)(phen)]	3000-3600(mbr) 3432(m)	–	1607(s)	1544(s)	1276(w)	1039(m)	580(m)	661(w)

In the complexes **2-7**, a new medium to weak intensity bands have occurred in the region 665-661 cm^{-1} that are attributable to arise due to in-plane ring deformation mode of pyridine bases indicative of their coordination to the metal centre [39]. The medium broad band that appears at 3440 cm^{-1} in complex **1** appears to have a contribution from coordinated water molecule [24,37] and the lattice water molecule while the broad band in the region 3600-3000 cm^{-1} in the complexes **2-5** appears to have a contribution from a lattice water molecule [40].

Cyclic voltammetry: The cyclic voltammograms of 2 mmol solutions of the ligand and complexes **1-3** in DMSO solvent under dinitrogen with 0.1 mol L^{-1} TBAP as a supporting electrolyte were studied. The values are given in Table-5 at a scan rate of 100 mV/s. The free ligand exhibits two quasi-reversible redox couples at -0.37 V ($E_{1/2}$) (ΔE = 260 mV) and +0.99 V ($E_{1/2}$) (ΔE = 100 mV) and an irreversible anodic peak potential at +0.83 V as shown in Fig. 4. The complexes do not show any metal-centered redox cycle (Fig. 4). The ligand-centered, oxidative and reductive waves that appear in the complexes are shifted from their original position in the ligand [41-43].

TABLE-5
ELECTROCHEMICAL DATA FOR THE LIGAND AND ITS Mn(IV) COMPLEXES (Pot. *vs.* Ag/AgCl) AT A SCAN RATE OF 100 mV/s

Ligand/Complex	Anodic peak potential, Epa (V)	Cathodic peak potential, Epc (V)
$slghH_4$	-0.24	-0.50
	+0.83	
	+1.04	+0.95
$[Mn^{IV}(slgh)(H_2O)_2]\cdot H_2O$ (**1**)	-0.275	-0.46
	+0.83	
	+1.10	+0.93
$[Mn^{IV}(slgh)(py)_2]\cdot H_2O$ (**2**)	-0.25	-0.47
	+0.83	
	+1.10	+0.94
$[Mn^{IV}(slgh)(2\text{-pic})_2]\cdot H_2O$ (**3**)	-0.22	-0.49
	+0.83	
	+1.10	+0.95

Antibacterial activity: The observed inhibitory zone against different bacteria were determined and listed in Table-6. The results show that the ligand has higher antibacterial activity against the two selected Gram-positive bacteria *Staphylococcus epidermis* and *Bacillus cereus* and one Gram-negative bacteria *Proteus vulgaris*. Complexes **2**, **6** and **7** have not shown any antibacterial activity against any of the tested bacteria *Bacillus cereus*, *Staphylococcus epidermis*, *Escherichia coli* and *Proteus vulgaris*. The complex **3** exhibited potent antibacterial activity against the Gram-positive bacteria *Staphylococcus epidermis* and Gram-negative bacteria *Escherichia coli* [3,23,26].

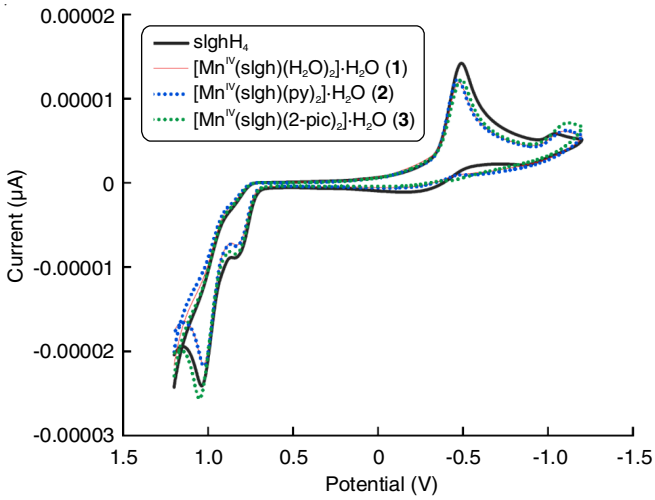

Fig. 4. Cyclic voltammogram of ligand (a) $slghH_4$ and complexes (b) $[Mn^{IV}(slgh)(H_2O)_2]\cdot H_2O$ (**1**), (c) $[Mn^{IV}(slgh)(py)_2]\cdot H_2O$ (**2**) and (d) $[Mn^{IV}(slgh)(2\text{-pic})_2]\cdot H_2O$ (**3**)

Conclusion

A series of new mononuclear manganese(IV) complexes derived from disalicylaldehyde glutaryldihydrazone were synthesized and characterized. The electron-rich deprotonated ligand can stabilize the high oxidation state of manganese. Consequently, the features of multidentate ligand have enabled the stabilization of the manganese in its high oxidation state. The dihydrazone functions as a tetradentate ligand and incorporates NNOO donors to coordinate Mn(IV) ions. The dihydrazone is present in enol form in these complexes and provides a coordination environment where the donors are arranged around manganese in the equatorial plane while the axial positions are occupied by water/pyridine/2-picoline/3-picoline/4-picoline in complexes **1-5**. In complexes **6** and **7**, the nitrogens from azomethine and 2,2′-bipyridine or 1,10-phenanthroline are in the equatorial positions, while the phenolate oxygens are in axial positions. The binding is through azomethine nitrogens and phenolate oxygens of both the hydrazone arms of the same dihydrazone that coordinate to the same metal center introducing steric crowding. Hence, one hydrazone arm remains in the equatorial plane while the other hydrazone arm is axial.

TABLE-6
ANTIMICROBIAL STUDIES OF THE LIGAND $slghH_4$ AND ITS MANGANESE(IV) COMPLEXES

Schiff base/complexes	Zone of inhibition (nm)			
	Gram-positive bacteria		Gram-negative bacteria	
	Staphylococcus epidermis	*Bacillus cereus*	*Escherichia coli*	*Proteus vulgaris*
$slghH_4$	15.91^{+++}	21.7^{+++}	–	24^{+++}
$[Mn^{IV}(slgh)(py)_2]\cdot H_2O$ (**2**)	–	–	–	–
$[Mn^{IV}(slgh)(2\text{-pic})_2]\cdot H_2O$ (**3**)	11^{+++}	–	10^{+++}	–
$[Mn^{IV}(slgh)(bpy)]$ (**6**)	–	–	–	–
$[Mn^{IV}(slgh)(phen)]$ (**7**)	–	–	–	–

Highly active = +++ (inhibition zone > 8.2 mm); moderately active = ++ (inhibition zone > 5.0-8.2); slightly active = + (inhibition zone > 2.5-5.0 mm); Inactive = – (inhibition zone < 2.5 mm).

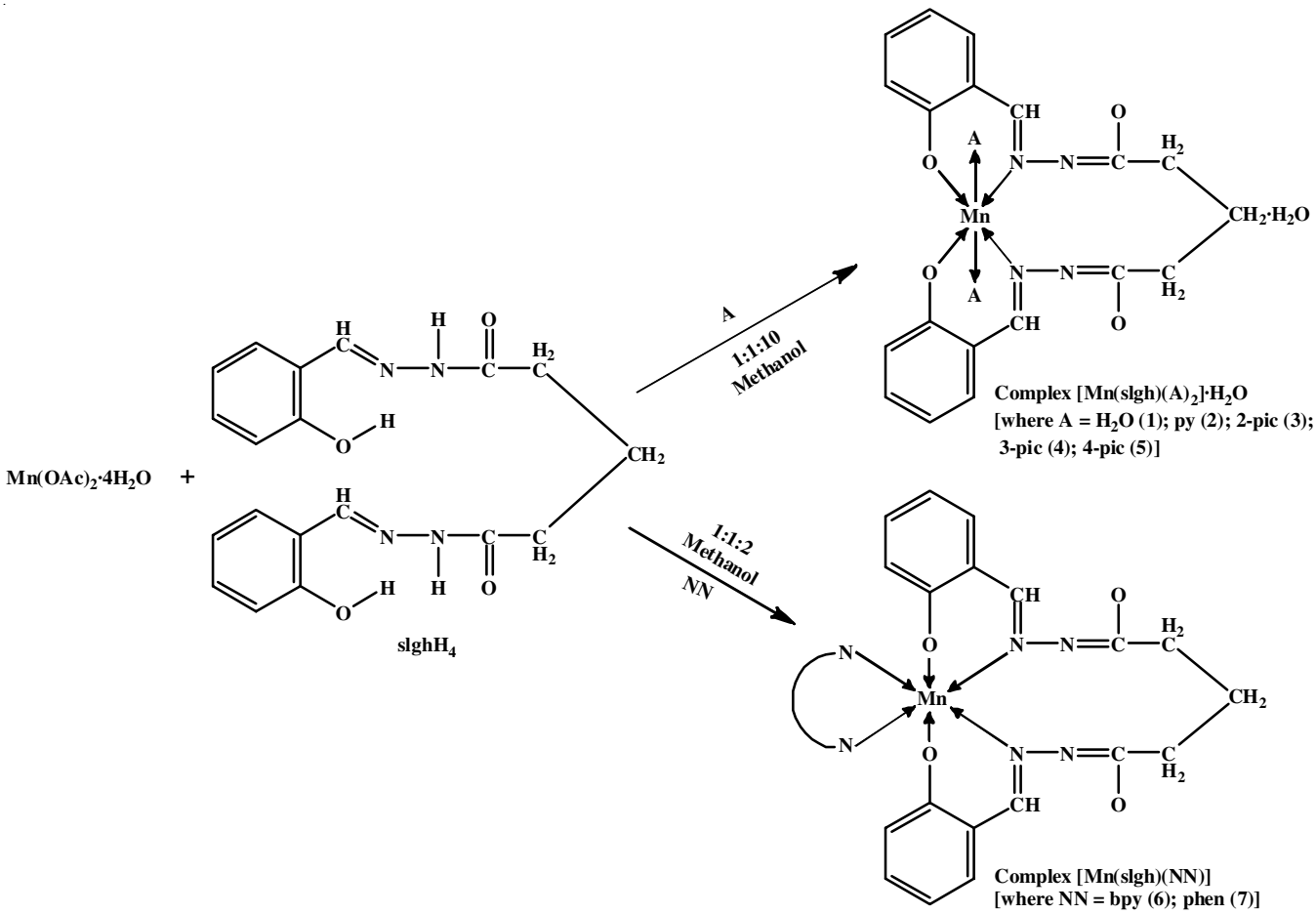

Fig. 5. Scheme of the reactions and structures of Mn(IV) complexes

In such configuration, axial azomethine absorbs at a lower frequency than equatorial azomethine as observed vaguely in IR spectra. Thus, the ligand is suggested to be coordinated to manganese in an *anti-cis* configuration. The enolate oxygens remain uncoordinated. The magnetic susceptibility data in all cases support the electronic and EPR data suggesting a Mn(IV) ion in octahedral stereochemistry in the complexes. Almost invariant redox potentials in the complexes are consistent with ligand-centered redox activity. The antibacterial studies confirmed that ligand shows more efficacy against two Gram-positive bacteria *Staphylococccus epidermis* and *Bacillus cereus* and one Gram-negative bacteria *Proteus vulgaris*. Complex **3** have been found more potent against one Gram-positive bacteria *Staphylococccus epidermis* and one Gram-negative-bacteria *Escherichia coli* while the other complexes **2**, **6** and **7** have not shown any antibacterial activity. The tentative structures of the mononuclear manganese(IV) complexes are presented in Fig. 5.

ACKNOWLEDGEMENTS

Two of the authors PS and PM are thankful to MHRD Government of India for research associate offered under the TEQIP-III project.The authors are thankful to Prof. R.A. Lal, Department of Chemistry, North-Eastern Hill University, Shillong, India and Prof. V. Manivannan, Department of Chemistry, IIT Guwahati, Guwahati, India for discussion and help. Thanks are also due to the CIF, IIT Guwahati, India for elemental analysis and EPR spectral data.

CONFLICT OF INTEREST

The authors declare that there is no conflict of interests regarding the publication of this article.

REFERENCES

1. A. Mumtaz, T. Mahmud and E. Mr, *J. Nucl. Med. Radiat. Ther.*, **7**, 1000310 (2016); https://doi.org/10.4172/2155-9619.1000310
2. R. Bikas, M. Ghorbanloo, R. Sasani, I. Pantenburg and G. Meyer, *J. Coord. Chem.*, **70**, 819 (2017); https://doi.org/10.1080/00958972.2017.1281918
3. A. Zülfikaroglu, Ç. Yüksektepe Ataol, E. Çelikoglu, U. Çelikoglu and Ö. Idil, *J. Mol. Struct.*, **1199**, 127012 (2020); https://doi.org/10.1016/j.molstruc.2019.127012
4. P. Ghosh, S.K. Dey, M.H. Ara and K. Md, *Egypt. J. Chem.*, **62**, 523 (2019); https://doi.org/10.21608/ejchem.2019.13741.185
5. R. Bhaskar, N. Salunkhe, A. Yaul and A. Aswar, *Spectrochim. Acta A Mol. Biomol. Spectrosc.*, **151**, 621 (2015); https://doi.org/10.1016/j.saa.2015.06.121
6. M. Sharma, K. Chauhan, R.K. Srivastava, S.V. Singh, K. Srivastava, J.K. Saxena, S.K. Puri and P.M.S. Chauhan, *Chem. Biol. Drug Des.*, **84**, 175 (2014); https://doi.org/10.1111/cbdd.12289

7. S. Carvalho, E. da Silva, R. Santa-Rita, S. de Castro and C. Fraga, *Bioorg. Med. Chem. Lett.*, **14**, 5967 (2004); https://doi.org/10.1016/j.bmcl.2004.10.007
8. R.A. Lal, D. Basumatary, A.K. De and A. Kumar, *Transition Met. Chem.*, **32**, 481 (2007); https://doi.org/10.1007/s11243-007-0189-3
9. R. Fekri, M. Salehi, A. Asadi and M. Kubicki, *Inorg. Chim. Acta*, **484**, S0020 (2018); https://doi.org/10.1016/j.ica.2018.09.022
10. M.S. Refat, S.A. El-Korashy, D.N. Kumar and A.S. Ahmed, *Spectrochim. Acta A Mol. Biomol. Spectrosc.*, **70**, 898 (2007); https://doi.org/10.1016/j.saa.2007.10.005
11. M.F.R. Fouda, M.M. Abd-Elzaher, M.M. Shakdofa, F.A. El-Saied, M.I. Ayad and A.S. El Tabl, *J. Coord. Chem.*, **61**, 1983 (2008); https://doi.org/10.1080/00958970701795714
12. A.S. El-Tabl, F.A. El-Saied, W. Plass and A.N. Al-Hakimi, *Spectrochim. Acta A Mol. Biomol. Spectrosc.*, **71**, 90 (2008); https://doi.org/10.1016/j.saa.2007.11.011
13. T. Matsushita, L. Spencer and D.T. Sawyer, *Inorg. Chem.*, **27**, 1167 (1988); https://doi.org/10.1021/ic00280a016
14. M. Retegan, V. Krewald, F. Mamedov, F. Neese, W. Lubitz, N. Cox and D.A. Pantazis, *Chem. Sci.*, **7**, 72 (2016); https://doi.org/10.1039/C5SC03124A
15. A. Harriman, *Coord. Chem. Rev.*, **28**, 147 (1979); https://doi.org/10.1016/S0010-8545(00)82012-3
16. Y. Gultneh, T.B. Yisgedu, Y.T. Tesema and R.J. Butcher, *Inorg. Chem.*, **42**, 1857 (2003); https://doi.org/10.1021/ic020131w
17. G.C. Dismukes, *Chem. Rev.*, **96**, 2909 (1996); https://doi.org/10.1021/cr950053c
18. M.W. Lynch, D.N. Hendrickson, B.J. Fitzgerald and C.G. Pierpont, *J. Am. Chem. Soc.*, **106**, 2041 (1984); https://doi.org/10.1021/ja00319a023
19. C.R. Lucas, K. Mitra, S. Biswas, S.K. Chattopadhyay and B. Adhikary, *Transition Met. Chem.*, **30**, 185 (2005); https://doi.org/10.1007/s11243-004-3225-6
20. M.K. Singh, B. Paul and A. Das, *ISOR J. Appl. Chem.*, **9**, 42 (2016).
21. A.I. Vogel, A Textbook of Quantitative Inorganic Analysis including Elementary Instrumentation Analysis, Longmans: London, Ed. 4 (1978).
22. M.S. Nair, D. Arish and R.S. Joseyphus, *J. Saudi Chem. Soc.*, **16**, 83 (2012); https://doi.org/10.1016/j.jscs.2010.11.002
23. R. Pal, V. Kumar, A.K. Gupta, V. Beniwal and G.K. Gupta, *Med. Chem. Res.*, **23**, 4060 (2014); https://doi.org/10.1007/s00044-014-0986-0
24. R.A. Lal, D. Basumatary, O.B. Chanu, A. Lemtur, M. Asthana, A. Kumar and A.K. De, *J. Coord. Chem.*, **64**, 300 (2011); https://doi.org/10.1080/00958972.2010.542238
25. B. Bouzerafa, D. Aggoun, Y. Ouennoughi, A. Ourari, R. Ruiz-Rosas, E. Morallon and M.S. Mubarak, *J. Mol. Struct.*, **1142**, 48 (2017); https://doi.org/10.1016/j.molstruc.2017.04.029
26. R.P. Bakale, G.N. Naik, S.S. Machakanur, C.V. Mangannavar, I.S. Muchchandi and K.B. Gudasi, *J. Mol. Struct.*, **1154**, 92 (2018); https://doi.org/10.1016/j.molstruc.2017.10.035
27. W.H. El-Shwiniy, W.S. Shehab and W.A. Zordok, *J. Mol. Struct.*, **1199**, 126993 (2020); https://doi.org/10.1016/j.molstruc.2019.126993
28. M.J. Camenzind, F.J. Hollander and C. Hill, *Inorg. Chem.*, **22**, 3776 (1983); https://doi.org/10.1021/ic00167a021
29. C.P. Pradeep, P.S. Zacharias and S.K. Das, *J. Chem. Sci.*, **118**, 311 (2006); https://doi.org/10.1007/BF02708524
30. J.R. Hartman, B.M. Foxman and S.R. Cooper, *Inorg. Chem.*, **23**, 1381 (1984); https://doi.org/10.1021/ic00178a017
31. A.B.P. Lever, Inorganic Electronic Spectroscopy, Elsevier: Amsterdam, New York, Ed.: 2 (1984).
32. S.K. Chandra and A. Chakravorty, *Inorg. Chem.*, **31**, 760 (1992); https://doi.org/10.1021/ic00031a013
33. R.A. Lal, S. Adhikari, A. Kumar, J. Chakraborty and S. Bhaumik, *Synth. React. Inorg. Chem.*, **32**, 81 (2002); https://doi.org/10.1081/SIM-120013148
34. O. Pouralimardan, A.C. Chamayou, C. Janiak and H. Hosseini-Monfared, *Inorg. Chim. Acta*, **360**, 1599 (2007); https://doi.org/10.1016/j.ica.2006.08.056
35. N.K. Chaudhary and P. Mishra, *Bioinorg. Chem. Appl.*, **2017**, 6927675 (2017); https://doi.org/10.1155/2017/6927675
36. D. Sadhukhan, A. Ray, G. Pilet, G.M. Rosair, E. Garribba, A. Nonat, L.J. Charbonnière and S. Mitra, *Bull. Chem. Soc. Jpn.*, **84**, 764 (2011); https://doi.org/10.1246/bcsj.20110004
37. M.K. Singh, N.K. Kar and R.A. Lal, *J. Coord. Chem.*, **62**, 1677 (2009); https://doi.org/10.1080/00958970802676649
38. X.-H. Lu, Q.-H. Xia, H.-J. Zhan, H.-X. Yuan, C.-P. Ye, K.-X. Su and G. Xu, *J. Mol. Catal. Chem.*, **250**, 62 (2006); https://doi.org/10.1016/j.molcata.2006.01.055
39. N. Nishat, T. Ahamad, S. Ahmad and S. Parveen, *J. Coord. Chem.*, **64**, 2639 (2011); https://doi.org/10.1080/00958972.2011.570754
40. P. Sarma, P. Mahanta, D. Basumatary and C. Medhi, *Asian J. Chem.*, **33**, 1144 (2021); https://doi.org/10.14233/ajchem.2021.23162
41. D.P. Kessissoglou, X. Li, W.M. Butler and V.L. Pecoraro, *Inorg. Chem.*, **26**, 2487 (1987); https://doi.org/10.1021/ic00262a030
42. P.J. Chirik and K. Wieghardt, *Science*, **327**, 794 (2010); https://doi.org/10.1126/science.1183281
43. M.D. Ward and J.A. Mc Cleverty, *J. Chem. Soc., Dalton Trans.*, **3**, 275 (2002); https://doi.org/10.1039/b110131p